INTERNATIONAL JOURNAL OF HYDROGEN ENERGY 45 (2020) 25509–25522

Available online at www.sciencedirect.com

ScienceDirect

journal homepage: www.elsevier.com/locate/he

A detailed investigation of the effect of hydrogen on the mechanical response and microstructure of Al 7075 alloy under medium strain rate impact loading

Burak Bal [a,*], *Bilge Okdem* [a], *Ferdi Caner Bayram* [a], *Murat Aydin* [b]

[a] *Department of Mechanical Engineering, Abdullah Gül University, 38080 Kayseri, Turkey*
[b] *Department of Aeronautical Engineering, Erciyes University, 38039 Kayseri, Turkey*

HIGHLIGHTS

- Hydrogen embrittlement is observed under impact loading.
- Impact toughness and ductility are degraded by hydrogen charging.
- Coexistence of several hydrogen embrittlement mechanisms is observed.
- Atomistic simulations are performed to better understand embrittlement mechanisms.
- Hydrogen increases the avarage dislocation mobility and reduces the cohesive energy.

ARTICLE INFO

Article history:
Received 27 April 2020
Received in revised form
10 June 2020
Accepted 24 June 2020
Available online 28 July 2020

Keywords:
Aluminum 7075
Mechanical testing
Impact test
Hydrogen embrittlement
Microstructure
Molecular dynamics

ABSTRACT

Effects of hydrogen and temperature on impact response and corresponding microstructure of aluminum (Al) 7075 alloy were investigated under medium strain rate impact loading. The specimens were subjected to impact energy of 12 J and 25 J, corresponding to impact velocities of 2.13 m/s and 3.08 m/s, respectively. These energy levels were decided after a couple of impact tests with different impact energy values, such as 6 J, 10 J, 12 J, 25 J. The experiments were conducted at five different temperatures. Electrochemical charging method was used for hydrogen charging. Microstructural observations of hydrogen uncharged and hydrogen charged specimens were carried out by scanning electron microscope. Hydrogen changed the crack propagation behavior of Al 7075 alloy depending on the temperature. Coexistence of several hydrogen embrittlement mechanisms, such as hydrogen enhanced decohesion (HEDE) and hydrogen enhanced localized plasticity (HELP) were observed under impact loading. The impact response of Al 7075 was significantly deteriorated by the hydrogen charging and changing temperature affected the absorbed energy of hydrogen-charged specimens. In addition, molecular dynamics simulations were conducted to uncover the atomistic origin of hydrogen embrittlement mechanisms under impact loading. In particular, hydrogen decreased the cohesive energy and enhanced the average dislocation mobility. Therefore, the experimental results presented herein constitute an efficient guideline for the usage of Al alloys that are subject to impact loading in service in a wide range of temperatures.

* *Corresponding author.*
E-mail address: burak.bal@agu.edu.tr (B. Bal).
https://doi.org/10.1016/j.ijhydene.2020.06.241

Introduction

Owing to a good combination of high strength to weight ratio, high corrosion resistance, reasonable ductility, and good machinability, the 7000 series aluminum (Al) alloys are attractive materials for extensive application areas such as defense, marine, military, aerospace and automotive [1–5]. When compared to other 7000 series, Al 7075, which has a face-centered cubic (FCC) crystal structure at room temperature, has the highest strength and fracture toughness in the T651 heat-treated condition [1,6]. The major element of Al 7075, zinc, together with heat treatment process, including solution treatment, stress relief by stretching and artificial aging, provides improved mechanical properties [3,7–9]. Specifically, artificial aging causes grain refinements with enhanced mechanical properties due to the coexistence of different hardening mechanisms such as solute solution hardening, precipitation hardening and dislocation hardening [10–12]. In addition, due to its stable FCC crystal structure at room temperature, hydrogen diffusion in Al lattice is low compared to that of body-centered cubic (BCC) crystal structure. In particular, hydrogen diffusivity in Al 7075 lattice is around 10^{-12} m^2/s [13]. Therefore, it can be used in hydrogen-related infrastructures. For instance, the materials of choice for high-pressure gas containers to store hydrogen are aluminum alloys or stainless steels [13]. On the contrary, it has also been shown that they are vulnerable to hydrogen embrittlement (HE) [14–16], whose occurrence is linearly proportional with the strength of a material, so the aforementioned strengthening mechanisms also enhance its susceptibility to HE. Thus, it is necessary to investigate the effect of hydrogen under different loading scenarios for the sake of their safe and reliable usage in hydrogen-related infrastructures.

It is a well-known fact that atomic hydrogen degrades the mechanical properties of high strength metallic materials [5,17–22] and change the nature of microstructural activities under different loading conditions [23–25]. However, the exact mechanism of HE is still unclear [26–29]. The proposed HE mechanisms, based on both experimental observations and numerical calculations, are hydrogen enhanced localized plasticity (HELP) [30,31], hydrogen enhanced decohesion (HEDE) [32,33] and adsorption-induced dislocation emission (AIDE) [14,33–35]. These mechanisms can be activated individually as well as they can be observed simultaneously depending on the loading conditions. The main HE mechanism of aluminum alloys has also been investigated widely under several conditions [13,14,16,36–46]. In these studies, it has been reported that Al alloys can absorb hydrogen during the homogenization process or service in aggressive environments [14,42,47,48]. Once hydrogen is diffused into the lattice, it can be localized at either trap sites or lattice sites, diffusible hydrogen [49,50]. Hydrogen diffusion, localization and interaction with dislocations in Al 7075 were investigated via uniaxial tensile tests at a strain rate of 10^{-5} s^{-1} at 318 K [13] as well as the correlation between hydrogen content and hardness and corrosion behavior of Al 7075 [51,52]. In addition, the effect of loading and microstructural factors on HE susceptibility of Al 7075 was investigated under tensile loading as well as the effect of hydrogen on the crack morphology and crack growth rate under cyclic loading [5,42,45,53]. However, despite the high amount of studies on the HE susceptibility of Al 7075, these works were carried out at low strain rates. In fact, most of the works on HE have been conducted under static or dynamic tensile/compressive loadings at low strain rates in order to provide enough time for hydrogen-dislocation interactions [20,54]. On the contrary, given the fact that materials can be subject to medium/high strain rates impact loadings during operation, the effect of hydrogen on the mechanical response and microstructure under impact loading at different strain rates should be investigated. As Al 7075 is one of the most utilized high strength materials in many different applications, determination of hydrogen effect at high strain rates is of utmost importance for the sake of their reliable usage. To the best of the authors' knowledge, a comprehensive study on the HE susceptibility of Al 7075 at several different medium strain rate impact loadings has not been carried out yet. What is available in the literature is the mechanical response of hydrogen uncharged Al 7075 under different loading conditions, such as impact, ballistic and Split-Hopkinson, over a wide range of strain rate (until 10^4 s^{-1}) and temperature (from −200 °C to 600 °C) [4,6,55–58].

In the present study, mechanical responses and microstructural aspects of hydrogen-charged and hydrogen-uncharged Al 7075 alloys were investigated by Charpy impact testing at different strain rates and a wide temperature range: −45 °C–100 °C. Electrochemical charging method was used for hydrogen charging. Material characterization was carried out via X-ray powder diffraction (XRD) and energy-dispersive X-ray spectrometer (EDX). Impact energy and force data of hydrogen-charged and hydrogen-uncharged specimens were collected from the very first instance of the impact to fracture. The effect of hydrogen on the microstructure was investigated by scanning electron microscopy (SEM). Overall, the findings of the study presented herein open a new venue for the utility of Al 7075 alloy in different applications that might be subject to impact loading and especially their usage in critical application areas, such as hydrogen storage, as HE-resilient material.

Material and method

As received material

In the present study, the 7075-T651 aluminum alloy was investigated and its chemical composition is presented in Table 1. T651 heat treatment process includes solution treatment, stress relief by stretching and artificial aging at 120 °C for 24 h followed by air cooling. Dynamic recrystallization occurs as a result of the T651 heat treatment process and it allows the nucleation and growth of new grains [57]. The tested materials were all polycrystalline and initially featured a nearly random texture [58–60].

Charpy V-notched (CVN) impact samples with dimensions of 55 mm × 10 mm × 10 mm, featured a 45° notch with 0.25 mm radius and 2 mm depth, were cut utilizing electro-discharge machining (EDM). The specimen surfaces were

Table 1 – Chemical composition of the studied material (in wt. - %).

Zn	Mg	Cu	Fe	Si	Cr	Al
5.1	2.57	1.9	0.49	0.3	0.2	Balance

prepared by using conventional grinding and polishing metallographic equipment. After grinding using sandpaper with different grades (up to 1200 mesh), the specimens were polished using a series of diamond pastes and finally chemically polished with an HF:H_2O_2 = 1:10 solution to remove the oxide layer, residual stress and to obtain a defect-free surface.

Microhardness values (HV0.2) of the 7075 aluminum alloy specimens around the notch, where is the critical region for impact testing, were examined using a MICROBUL – 1000 D micro-hardness tester. The average Vickers hardness values, which are almost uniform, of undeformed Al 7075 samples were found as 182.2 H V. Uniform hardness values around the notch indicate a uniform microstructure. Bruker D8Discover X-ray diffractometer, operating at 40 kV and 40 mA with a Cu-Kα source (wavelength = 1.5406 Å), was used to perform the XRD analysis. Fig. 1a shows the XRD data of as-received + undeformed, as received + fractured and hydrogenated + fractured materials. The data were collected over a range of 0°–90° in 2θ and the XRD. Despite different intensities of all tested materials, the crystallographic planes are quite similar at Bragg angles of 38, 44, 65, 78 and 83° which correspond to (1 1 1), (2 0 0), (2 2 0), (3 1 1) and (2 2 2) reflections, respectively. Note that the XRD data were taken from close to the notch region of all specimens. The initial microstructure was also observed using scanning electron microscope (SEM, Zeiss Gemini 300, AGU - Central Research Facility) equipped with an energy dispersive X-ray spectrometer (EDX) and the corresponding results are given in Fig. 1b.

Hydrogen charging, impact tests, and microstructural characterization

Hydrogen was introduced into the specimens by an electrochemical charging process before impact tests at 353 K in an aqueous solution with 3% (mass %) NaCl consisting of 3 g/L ammonium thiocyanate (NH_4SCN) [20]. A platinum rod was used as the counter-electrode. The specimens were charged for 24 h at a current density of 50 A/m^2 and based on our numerical modeling in 1D and 2D, most of the hydrogen diffused up to 3 mm in depth throughout the thickness and with molecular dynamics modeling, it has been concluded that they tend to accumulate around notched region and change the impact response. The details of modeling are given in the final remarks section below. To observe the hydrogen effect at high strain rates and different temperature ranges, one set of the specimens was electrochemically charged with hydrogen. A schematic representation of our charging system was provided in the supplementary materials.

The impact tests were carried out with and without hydrogen charging at a wide variety of different temperature conditions including −45 °C, 0 °C, RT, 60 °C and 100 °C. The tests were carried out using an instrumental impact-testing

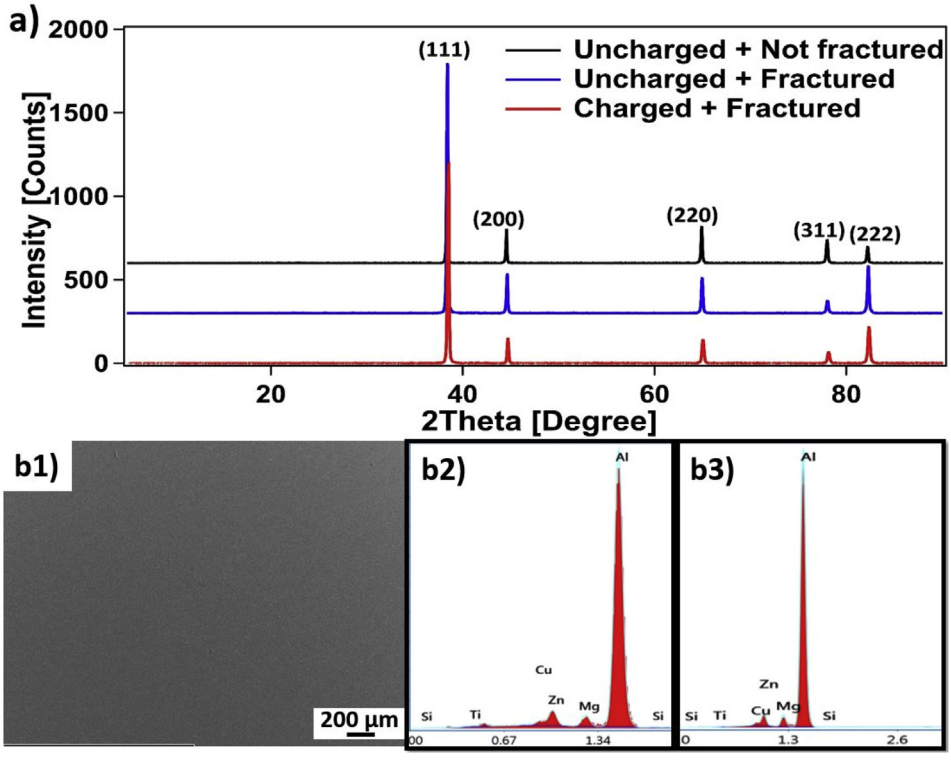

Fig. 1 – Characterization of the as received material (a) XRD results of tested Al 7075 specimens at three different conditions (b) SEM image and corresponding EDX results of tested Al 7075 alloy (undeformed, hydrogen uncharged) (b1) SEM image of the scanning area, EDX results for (b2) 10 kV, (b3) 20 kV.

machine in accordance with ASTM E23 specifications. Heating and cooling processes were carried out by using a furnace and liquid nitrogen, respectively. The temperatures during impact tests were recorded by a digital 2 k-type thermocouple. During cooling, specimens reached −45 °C and 0 °C in less than 45 s. At elevated temperatures, we have placed the hydrogen charged specimens into the furnace after the furnace reached the desired temperatures. Once the specimens reached the corresponding temperatures (within 30 min), the impact tests were conducted immediately after the specimens were taken away from the furnace. The specimens were subjected to impact energy of 12 J and 25 J, corresponding to impact velocities of 2.13 m/s and 3.08 m/s, respectively. These energy levels were decided after a couple of impact tests with different impact energy values, such as 6 J, 10 J, 12 J, 25 J. Specifically, 10 J and 12 J did not provide the necessary amount of energy for fracture of hydrogen-uncharged specimens at low temperatures and elevated temperatures, respectively, but 12 J impact energy was sufficient to fracture hydrogen-charged specimens at all temperatures. Therefore, minimum energy values, which can fracture both hydrogen-uncharged and hydrogen-charged specimens, were adjusted to perform the impact tests.

The fracture surfaces of the hydrogen-charged and hydrogen-uncharged specimens were examined by SEM (Zeiss Gemini 300) and EDX. The measurements were conducted at 5.00 kV using secondary electrons. Therefore, the effect of hydrogen on the microstructure was revealed under impact loading at different temperatures.

Results and discussion

Fractographic analysis

Various impact tests at different initial energy levels were conducted in order to specify the minimum amount of energy to perform the rest of experiments at different temperatures. In particular, minimum energy provided both the fracture and hydrogen embrittlement at the same time due to relatively moderate strain rate, which allows enough time for dislocation-hydrogen interactions. Fig. 2 shows some of the deformed and fractured specimens at different energy values and temperatures. Fig. 2a shows the fracture appearances of the hydrogen-uncharged specimens after impact tests. In particular, 10 J impact energy (Fig. 2a, top image) propagated the crack from the notch but could not break the specimen completely, however, a slight increase in the energy level to 12 J (Fig. 2a, bottom image) provided a complete failure. Specifically, 12 J provided enough energy to fracture all hydrogen-charged specimens at all temperatures. On the other hand, 12 J impact energy was not enough to fracture the hydrogen uncharged specimens at elevated temperatures, as shown in Fig. 2b. Especially, the specimen tested at 100 °C resist all the impact energy without noticeable macroscopic crack propagation (Fig. 2b, bottom image). On the contrary, significant macroscopic crack propagation was observed in the specimen tested at 60 °C (Fig. 2b, top image). The increase in the impact resistance with temperature is consistent with the literature and it is due to the ease of the dislocation movement and an increase in the kinetics and interaction of dislocations at elevated temperatures [61,62]. This way, the given energy to the specimen is used for microstructural activities, i.e. primary dislocation motion or forest dislocation nucleation, and corresponding plastic deformation instead of crack propagation [63,64]. In particular, once the stress concentration at the tip of a notch cannot be accommodated plastically by microstructural activities, the crack propagates. Thus, the stress concentration was accommodated plastically at 100 °C but the crack was propagated at 60 °C. Thus, the experiments at elevated temperatures were also carried out at 25 J impact energy which provided enough energy to fracture of hydrogen-uncharged specimens at 60 °C and 100 °C. On the other hand, 12 J impact energy could easily separate hydrogen-charged specimens into two at all temperatures. Two representative images are given in Fig. 2c. Top and bottom images show the hydrogen-charged specimens after impact at 60 °C and 100 °C, respectively.

Impact tests below room temperature

Fig. 3a and b shows the physical appearances of the CVN hydrogen uncharged (top) and hydrogen charged (bottom) specimens after the impact tests at −45 °C and 0 °C, respectively. The low temperature tests were conducted at 12 J and complete fracture was observed in all CVN specimens. Even though the crack was propagated directly through the central portions of hydrogen uncharged specimens, the fracture region of hydrogen charged specimens occurred at almost 45° to the direction of the impact loading at both temperatures. Figs 4 and 5 show the corresponding fracture morphologies of hydrogen-charged and hydrogen-uncharged specimens at −45 °C and 0 °C, respectively. Fig. 4b and d are higher magnification images taken from the fracture surfaces of each corresponding specimen. It can be observed clearly from SEM images that hydrogen promoted secondary cracks and deeper primary cracks compared to hydrogen-uncharged specimen under impact loading. Similar observations were also carried out previously [65]. In addition, transgranular crack (TC) propagation was observed at −45 °C (Fig. 4), whereas intergranular cracks (IC) were observed at 0 °C (Fig. 5). It is obvious that hydrogen diffusivity decreases with temperature [66,67]. Therefore, the interactions of hydrogen and dislocations may slow down in the course of dislocation slip [68]. In addition, decreasing temperature promotes hydrogen trapping [69] and also decreases the stacking fault energy, which triggers splitting of dislocations and causes high volume fraction of planer dislocations since the split dislocations possess a lower ability to cross slip. Therefore, split dislocations and resulting planer slip enhance sweeping of atomic hydrogen into trap regions [69]. Thus, hydrogen accumulation in the triaxial stress regions ahead of the crack tip reduces the cohesive energy and promotes deeper cracks and changes the fracture mode from dimple like to cleavage (Figs 4 and 5). Cleavage facets were sharper at lower temperature. Current results are in accordance with previous studies on the effect of hydrogen of the crack propagation behavior [25,70,71], At low temperatures, it has been observed that shear slip bands are the favorable places for dislocation transportation [68]. Therefore, another hydrogen accumulation region is the shear slip bands. Therefore, high hydrogen concentration in the localized shear

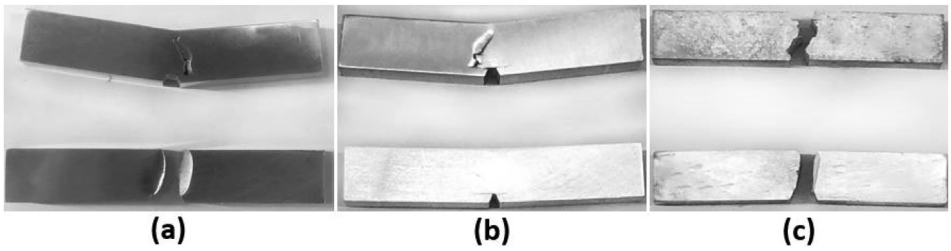

Fig. 2 – Image of the Al 7075 specimens after impact tests with (a) hydrogen uncharged at 10 J impact energy and RT (top) and 12 J impact energy (bottom) and RT (b) hydrogen uncharged at 12 J impact energy and 60 °C (top), at 100 °C (bottom), (c) hydrogen charged at 12 J impact energy and 60 °C (top), at 100 °C (bottom).

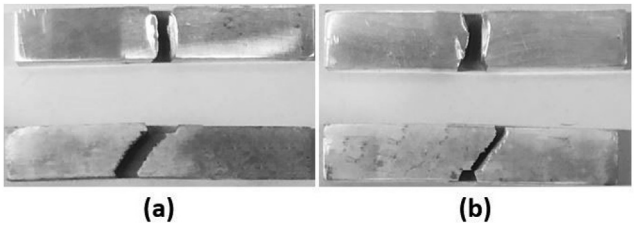

Fig. 3 – Physical appearances of the CVN hydrogen uncharged (top) and hydrogen charged (bottom) specimens after the impact tests at (a) −45 °C and (b) 0 °C.

slip band reduced the cohesive energy of the corresponding regions and the cracks were propagated with almost 45° to the direction of the impact loading (Fig. 3a and b, bottom images). In particular, aforementioned effect was more pronounced at lower temperature (−45 °C) and no similar result was observed at higher temperatures. Whereas, the crack was propagated directly along the impact direction in the hydrogen uncharged specimen (Fig. 3a and b, top images).

Impact tests at room temperature and above room temperature

Fig. 6a–c shows the physical appearances of the CVN hydrogen uncharged (top) and hydrogen charged (bottom) specimens after the impact tests at RT °C and 60 °C and 100 °C, respectively. It should be noted that all the hydrogen charged specimens were broken into two separate pieces under 12 J impact energy but hydrogen uncharged specimens at 60 °C and 100 °C were broken into two separate pieces under 25 J impact energy. Thus, it is obvious that hydrogen reduced the ductility of samples tested at elevated temperatures under impact loading, which is a well-known effect of hydrogen under tensile loading [19,72,73]. At room temperature and 100 °C primary cracks propagated directly along the impact direction but at 60 °C primary cracks propagated from the notch showed a zigzag path regardless of the hydrogen charging. This might be attributed to the short-range ordering

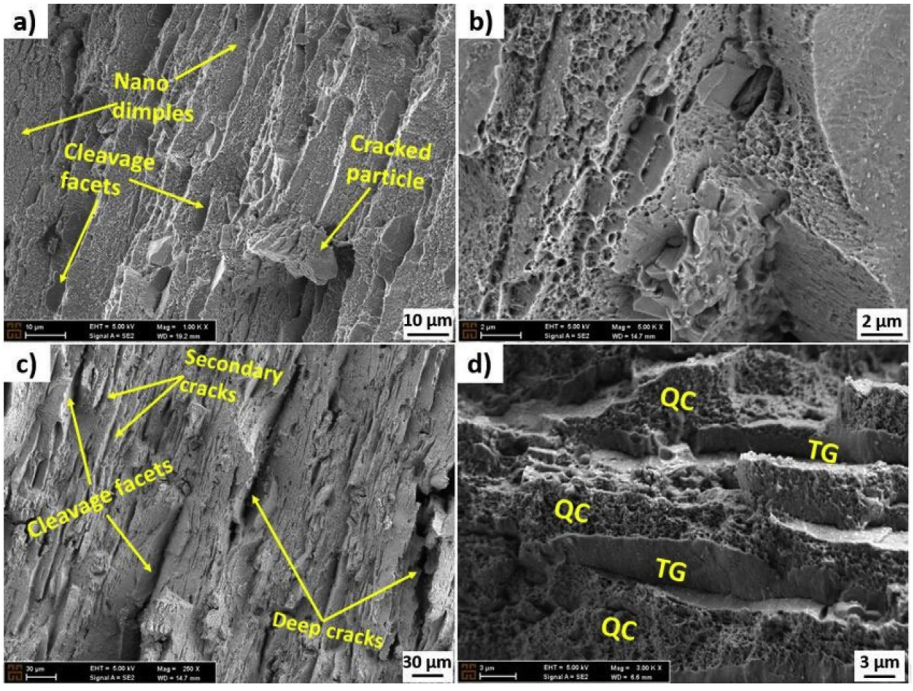

Fig. 4 – Fracture surface of the tested specimens at −45 °C (a) uncharged and (c) charged with hydrogen. (b) and (d) are the higher magnification images from (a) and (c), respectively.

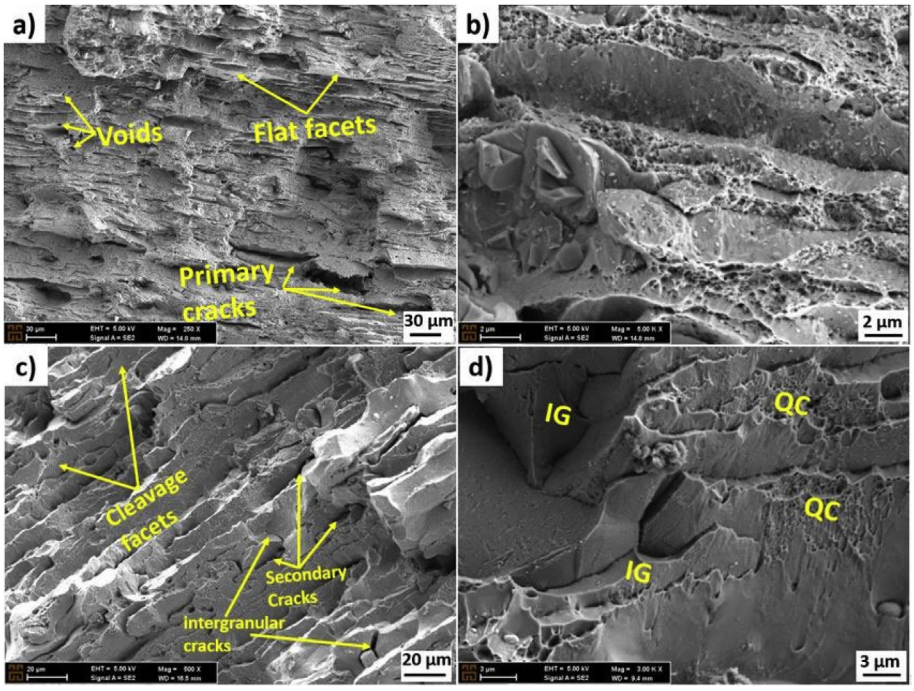

Fig. 5 – Fracture surface of the tested specimens at 0 °C (a) uncharged and (c) charged with hydrogen. (b) and (d) are higher magnification images of (a) and (c), respectively.

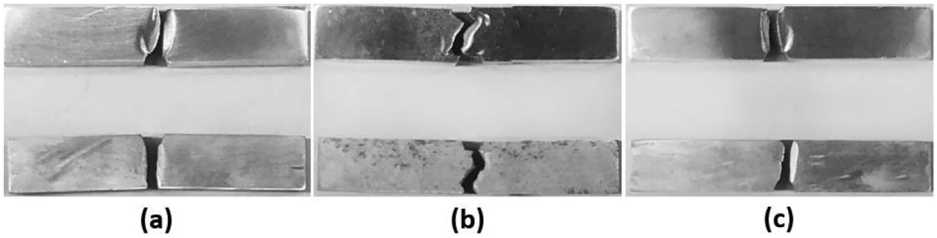

Fig. 6 – Physical appearances of the CVN hydrogen uncharged (top) and hydrogen charged (bottom) specimens after the impact tests at (a) RT, (b) 60 °C and (c) 100 °C.

induced by high Zn concentration in the chemical concentration, which can be promoted at critical temperatures and it assists planer slip [74]. However, further experimental observations together with numerical simulations have to be conducted to strengthen and prove the occurrence of short-range ordering at 60 °C. Thus, there were various nucleation sites and propagation routes of cracks at 60 °C regardless of the hydrogen charging. Fracture surfaces were observed by means of SEM after the impact tests and shown in Figs 7–9. Parts (b) and (d) are the higher magnification images taken from the fracture surfaces of each corresponding specimen. Cracks were initiated at the stress concentration regions and propagation behavior was changed from transgranular to intergranular by hydrogen charging at 60 °C (Fig. 8) which is consistent with the literature [75–77]. Voids, primary cracks, and nano-sized dimples, an indication of ductile fracture, were observed on the fracture surface of all the tested specimens regardless of the presence of hydrogen and temperature (Figs 7–9). However, the volume fraction of nano-sized dimples in the fracture surfaces of hydrogen uncharged specimens is greater than hydrogen-charged specimens at all temperatures. Therefore, HELP mechanism, which was pronounced at higher temperatures, might be activated during impact. On the contrary, the specimens charged with hydrogen had deeper cracks, even up to 200 μm, as well as several cleavage facets, indicating brittle fracture (Figs 7–9). Thus, the coexistence of HELP + HEDE mechanisms triggered mixed fracture mode in the hydrogen charged specimens. Similar observations were carried out previously [78–81]. In particular, if well-developed dimples and corresponding MVC features dominate the fracture surface, HELP becomes a dominant mechanism, whereas, if brittle fracture modes, i. e, quasi-cleavage (QC), TC and IC dominates the fracture surface HEDE is the dominant HE mechanism [33,78]. Simultaneous activation of MVC, TC/IC is shown in Figs 7–9. MVC represents the ductile fracture and corresponding localized plasticity (HELP) and cracks represent the brittle fracture (HEDE). Specifically, QC + TC + IC > MVC at room temperature, indicating that HEDE is more dominant HE mechanism at room temperature under impact loading. Moreover, both HELP and HEDE have been equally activated at 60 °C and HELP is the dominant HE mechanism at 100 °C. More SEM figures,

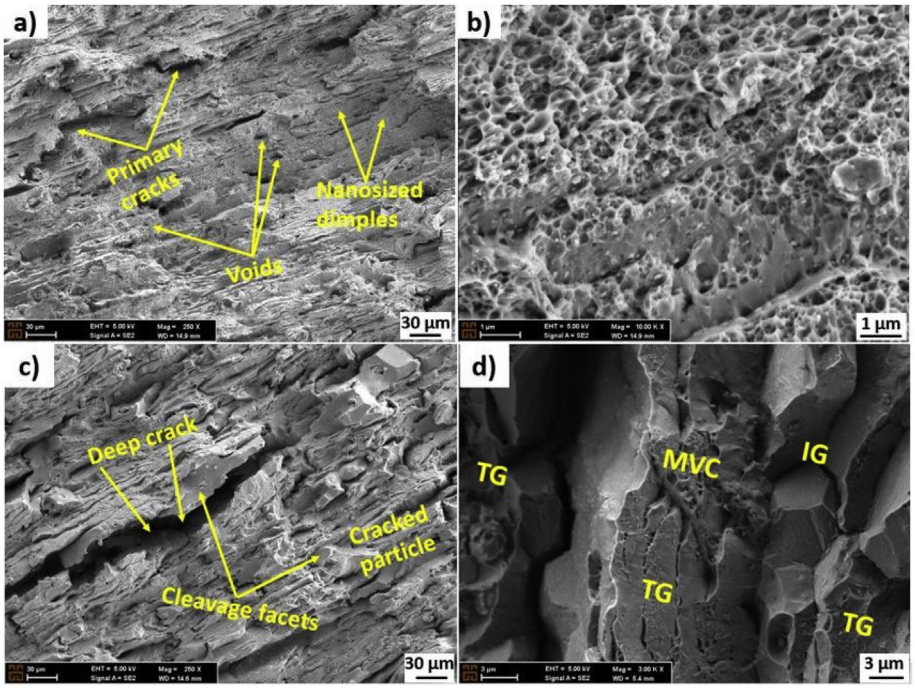

Fig. 7 – Fracture surface of the tested specimens at RT (a) uncharged and (c) charged with hydrogen. (b) and (d) are the higher magnification images from (a) and (c), respectively.

showing the coexistence of HELP + HEDE mechanisms were given in the supplementary materials. It can be clearly seen that the volume fraction of dimples increases with temperature (Figs 7–9). In addition, hydrogen caused the formation of secondary cracks and changed the crack propagation behavior as discussed above. Therefore, it can be concluded that 12 J impact energy, corresponding to 2.13 m/s impact velocity, was sufficient to promote HE at all temperatures.

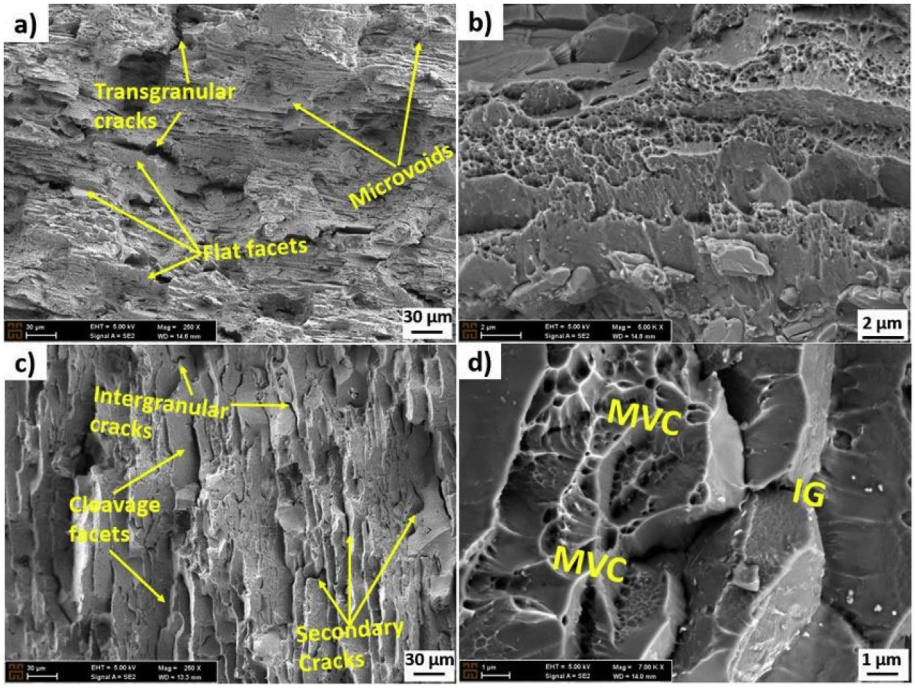

Fig. 8 – Fracture surface of the tested specimens at 60 °C (a) uncharged and (c) charged with hydrogen. (b) and (d) are the higher magnification images from (a) and (c), respectively.

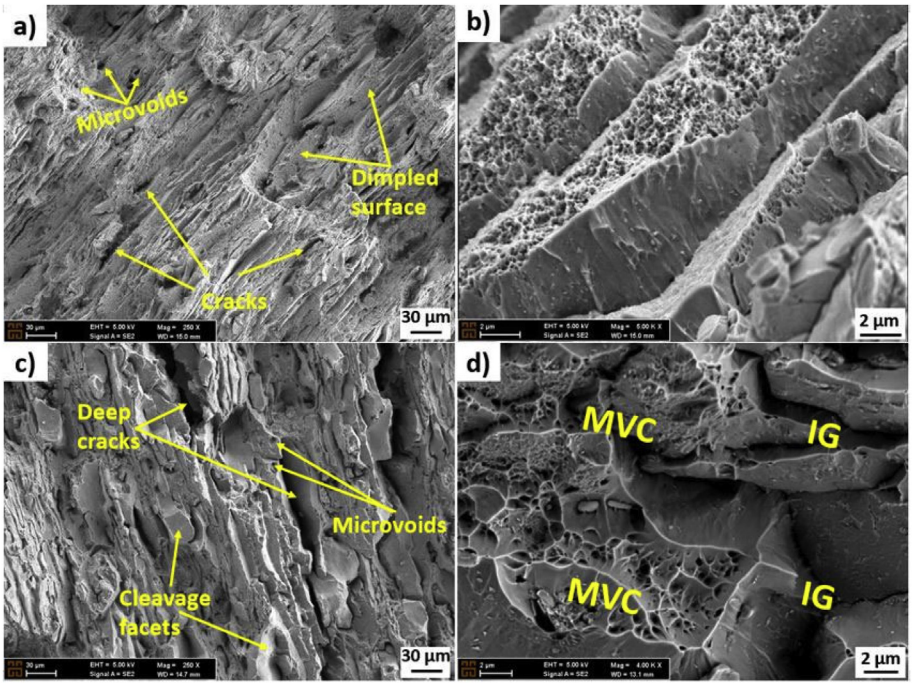

Fig. 9 – Fracture surface of the tested specimens at 100 °C (a) uncharged and (c) charged with hydrogen. (b) and (d) are the higher magnification images from (a) and (c), respectively.

Mechanical response analysis

Fig. 10 demonstrates the impact energy-time behavior of hydrogen-uncharged and hydrogen-charged Al 7075 samples at different temperatures and the corresponding absorbed energy results are shown in Fig. 10f as a function of test temperature. For hydrogen-uncharged specimens, the maximum absorbed energy was recorded at elevated temperatures (60 °C and 100 °C) since the mobility of dislocations increases with temperature and it allows specimens to absorb more energy for plastic deformation without fracturing. Likewise, the specimens could not absorb high-energy values at low temperatures owing to the fact that the nature of material turned into brittle since the movement of dislocations was hindered. Moreover, hydrogen decreased the impact energy and corresponding toughness of the tested specimens at all temperatures (Fig. 10). It is obvious that hydrogen made the tested specimens brittle and increasing temperature from −45 °C to RT did not change the absorbed impact energy of hydrogen-uncharged specimens considerably (from 6.56 J to 6.10 J), whereas it decreased the absorbed impact energy of hydrogen-charged specimens from 4.86 J to 2.39 J (Fig. 10f). In addition, hydrogen-charged Al 7075 alloys are brittle even at elevated temperatures under impact loading since they cannot absorb enough energy for plastic deformation. It is obvious that hydrogen decreased the time for fracture.

Fig. 11 shows the force versus time graphs of hydrogen-charged and hydrogen uncharged specimens at different temperatures. The oscillations that appeared during the impact tests were the first and second symmetric vibration modes, which were reported in the literature previously [55,82]. Regardless of the testing temperature, the presence of hydrogen significantly reduced the contact force of the specimens due to the weakening of interatomic bonds in the presence of hydrogen (HEDE). The sudden drop in force after a certain time can be attributed to the softening behavior after macro-crack propagation and associated with the new surface formation energy as soon as the macro-crack formation criterion was reached [83].

Final remarks

Hydrogen diffusion modeling

2D mass diffusion model was prepared in cartesian coordinates. Eq. (1) gives a transient diffusion of solutes in 2D to determine hydrogen concentration at a point defined with two principal coordinates at a specific time. $C_{x,y,t}$ is the normalized hydrogen concentration at given location in the bulk material at a specific time, t. $C_{x,y}$ was taken as 0 when $t < 0$ and 1 only for the surface edges when $t > 0$ as boundary conditions.

$$\frac{\partial C_{x,y,t}}{\partial t} = D^* \left[\frac{\partial^2 C_{x,y,t}}{\partial x^2} + \frac{\partial^2 C_{x,y,t}}{\partial y^2} \right] \quad (1)$$

where, D is the hydrogen diffusion coefficient, assumed to be constant at a given temperature.

No hydrogen trapping was considered and the hydrogen diffusion model in the HT metallurgical state (eq. (2)) was utilized in our diffusion model.

$$D = D_0 \exp\left[-\frac{E_a}{RT} \right] \quad (2)$$

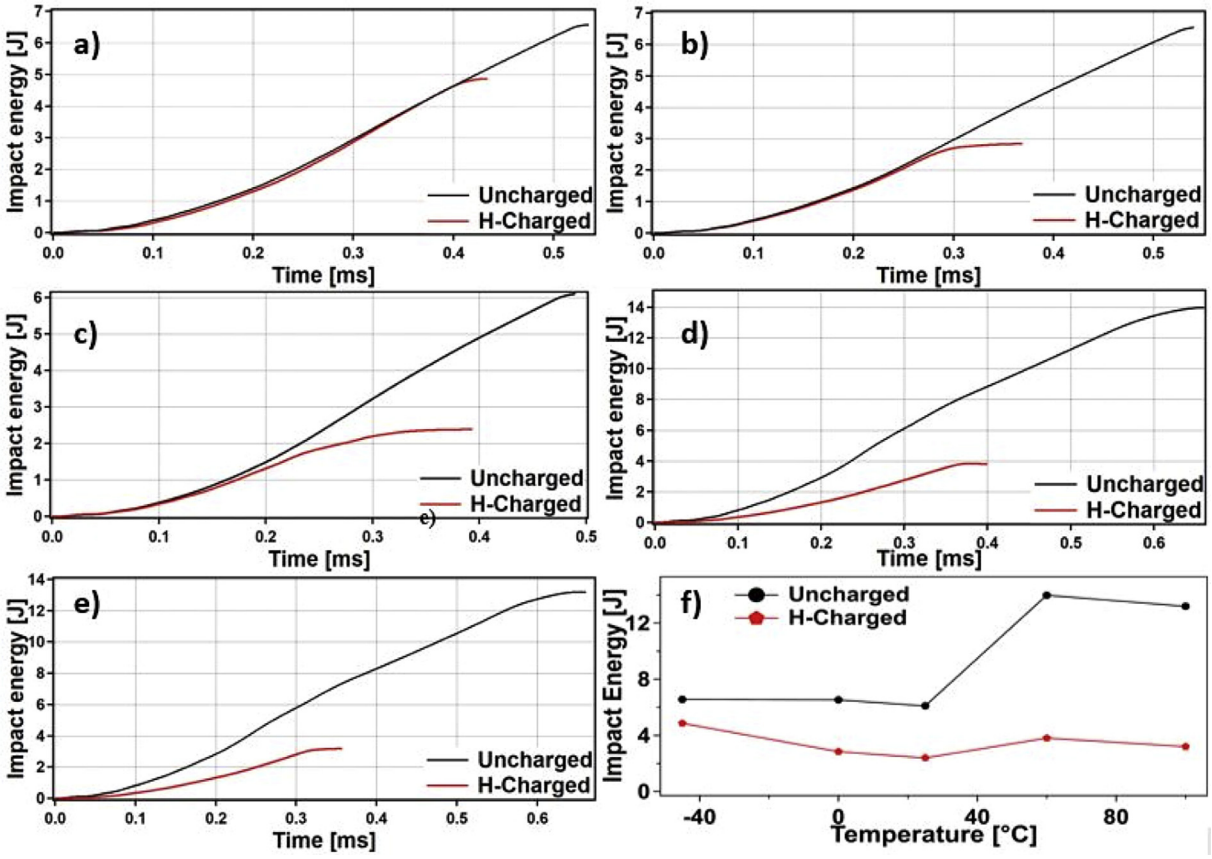

Fig. 10 – Impact energy - time graphs for experiments of hydrogen charged and uncharged conditions at different temperatures as (a) −45 °C (b) 0 °C (c) RT (d) 60 °C (e) 100 °C (f) Impact energy–temperature curve for the hydrogen charged and hydrogen-charged Al alloy investigated in this study.

where, D_0 is the pre-exponential factor and E_a is the effective activation energy for hydrogen diffusion. Summary of literature for effective diffusion parameters for Al 7XXX series, including Al 7075-T6, was given in the study of Scully et al. [84]. It should be noted that T6 tempering also increases the diffusivity [85]. In order to solve the above diffusion model (eq. (1)), a discretization method was utilized to avoid any round-off error and nodal solutions were found iteratively in an incremental manner via Eq. (3). In Eq. (3), d is defined as diffusion number, calculated through Eq. (4), where Δx represents the length increment for a nodal analysis and Δt is the time increment. Due to the natural symmetry of the model only Δx was used. A convergence analysis employed to find ideal d value.

$$C_{x,y,t+1} = C_{x,y,t} + d*\left[C_{x+1,y,t} + C_{x-1,y,t} + C_{x,y+1,t} + C_{x,y-1,t} - 4*C_{x,y,t}\right] \quad (3)$$

$$d = D*\frac{\Delta t}{\Delta x^2} \quad (4)$$

It is clearly seen that hydrogen diffused up to 3 mm in depth throughout the thickness after 24 h at 353 K. Very few fractions of hydrogen diffused even 3.8 mm in depth. Therefore, hydrogen could not reach up to the center of the specimen but reached into the subsurface and our charging conditions ensured that hydrogen diffusion length exceeds the initial notch depth (2 mm, Fig. 12a). The diffusion model corresponds well with results published in the literature [86,87].

The aforementioned hydrogen diffusion model was also used to simulate dehydrogenation at 60 °C and 100 °C. Hydrogen concentration after 24 h was utilized as new boundary conditions for the back-diffusion model. The relationship between temperature and diffusion coefficient was studied in the literature and the effect of temperature on the hydrogen diffusion coefficient was also taken into account in our back-diffusion model [84]. Fig. 12b and c shows the back-diffused hydrogen concentrations at 60 °C and 100 °C, respectively. It can be clearly seen from the figures that hydrogen back-diffusion occurs only at the surface and subsurface (max 0.5 mm in 30 min) and no significant back-diffusion from the specimen was observed. Therefore, heating the tested specimens up to desired temperatures before impact tests did not cause remarkable hydrogen loss.

Molecular dynamics modeling

Molecular dynamics (MD) simulations were conducted by LAMMPS (Large-scale Atomic/Molecular Massively Parallel Simulator) software in order to understand the atomistic origin of the observed HE mechanisms by monitoring the effects of atomic hydrogen on dislocation mobility and cohesive

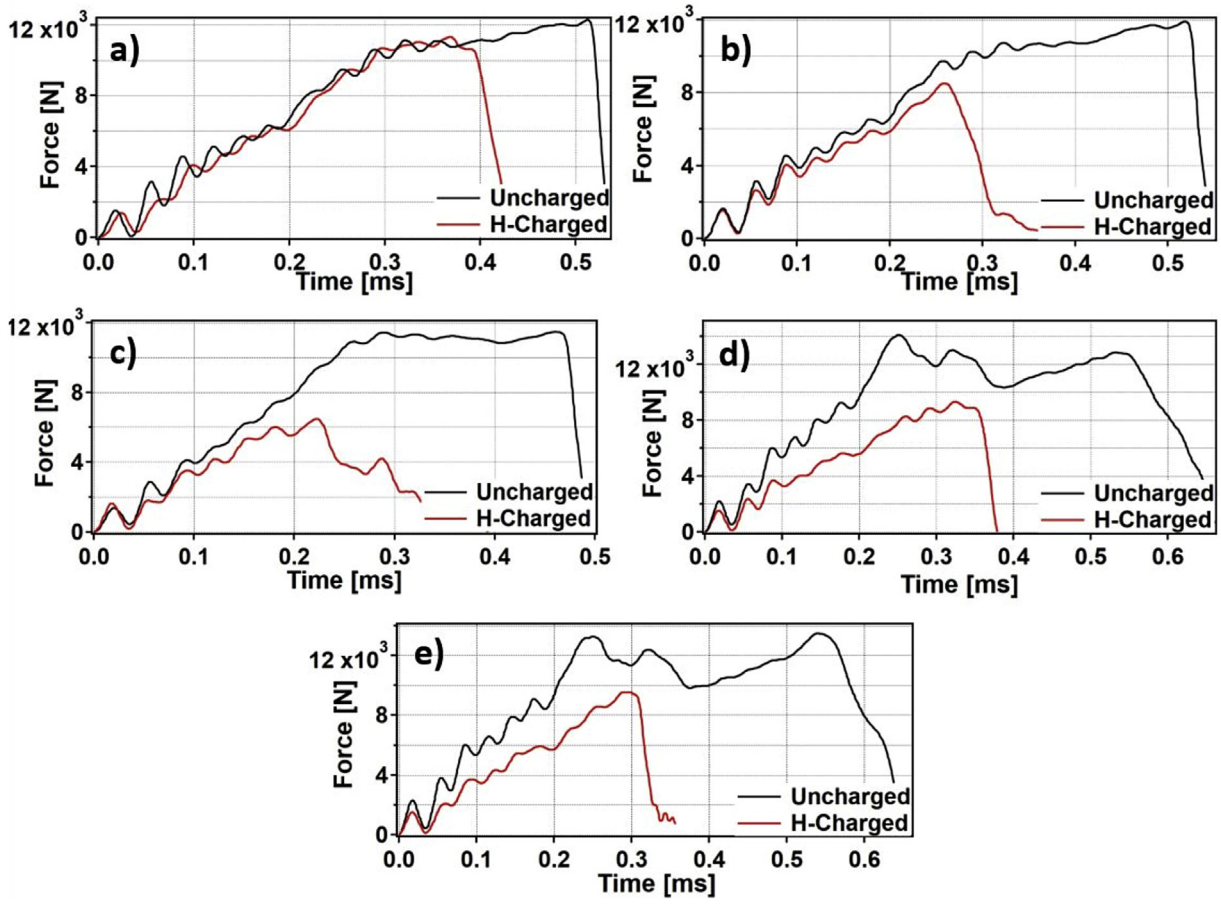

Fig. 11 – Experimental contact force histories of hydrogen charged and uncharged specimens at different temperatures as (a) −45 °C (b) 0 °C (c) RT (d) 60 °C (e) 100 °C.

energy. In particular, the simulations were conducted for 3 configurations: 1) Polycrystalline fcc aluminum (both hydrogen-uncharged and charged) with total number of 780.000 atoms and 16 randomly oriented grains were produced by Voronoi tessellation method and a 1 nm long central preexisting crack was formed by removing the atoms within 10 A° along y axis that corresponds to direction normal to the crack plane and MD simulations were carried out. From these simulations, it was observed that ½[110] edge dislocation generation arise from crack tips and grain boundaries during deformation. The initial atomic configuration snapshot of polycrystalline supercell was provided in the supplementary materials 2) In order to analyze the effect of hydrogen on the dislocation mobility, single ½[110] dislocation with burgers vector along the x direction containing supercells were generated with total number of 10.000 atoms. After an energy equilibration each supercell were loaded with 1.5 GPa transverse shear along y plane x direction. 3) A rectangular supercell containing 35.000 total number of atoms was used for the simulations with dimensions of 24 × 12 × 2 nm for x, y and z directions respectively and a 12 nm long central pre-existing crack was formed by removing the atoms within 12 A° along y axis that corresponds to direction normal to the crack plane. Periodic boundaries were used for all three directions. For the hydrogen-charged simulations, 0.0025 H/Al, 0.005 H/Al and 0.01 H/Al containing supercells were generated by randomly placing the hydrogen atoms into the initially generated supercell. Pair interactions between the Al–Al, H–H, and Al–H were defined by the second nearest-neighbor 2NN MEAM (modified embedded atom method) potential that developed by Ko et al. [88]. For both hydrogen uncharged and hydrogen charged Al simulations, energy equilibration was carried out by NVE ensemble (constant volume and energy) at 300 K and NPT ensemble (constant pressure and temperature) at 300 K and 0 isobaric pressure, after energy minimization. Both steps were carried out for 50 ps with 1 fs timestep. Afterwards, each supercell was deformed along y direction with a strain rate of 10^{-3} ps^{-1} (10^{9} s^{-1}) until the fracture occurs by using the same timestep. Polycrystalline structure and dislocation formations were analyzed by common neighbor analysis and dislocation extraction algorithm (DXA) [89] within the OVITO software [90].

The results of MD simulations were given in Fig. 12d–f. Fig. 12d shows the initial atomic configuration snapshot of the hydrogen-charged specimen, the snapshot was taken just after the relaxation. The green and blue atoms represent the aluminum and hydrogen atoms, respectively. It was observed that hydrogen addition enhanced the average dislocation mobility, that is well known observation in HELP mechanism (Fig. 12e). Dislocation mobility was determined from the

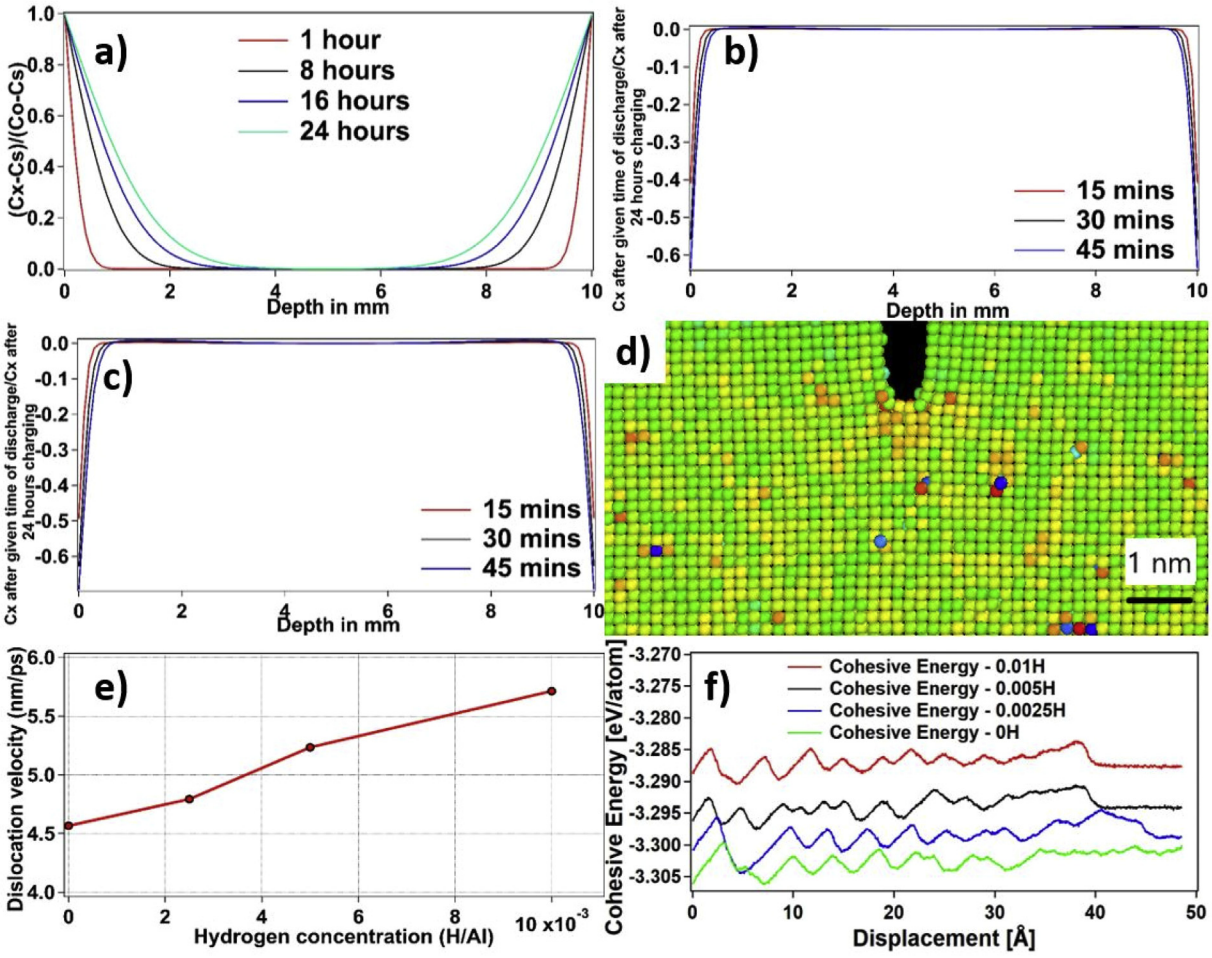

Fig. 12 – (a) Hydrogen diffusion profiles at 353 K for different charging times (b) back-diffused hydrogen concentrations at 60 °C (c) back-diffused hydrogen concentrations at 100 °C (d) Initial atomic snapshot of the hydrogen-charged specimen (e) effect of hydrogen on dislocation velocity (f) effect of hydrogen on cohesive energy.

position differences of dislocations at different steps. Moreover, it was observed that hydrogen enhanced dislocation nucleation near the crack tip during the deformation and triggered localized plasticity. In addition, hydrogen segregated around the crack during the deformation and decreased the cohesive energy (Fig. 12f), which is a common observation in HEDE mechanism. Specifically, as the hydrogen concentration increases, the cohesive energy decreases (Fig. 12f). These results align well with the previous MD studies [91–94]. Current set of MD modeling results strengthen the experimentally observed simultaneous activations of HELP and HEDE mechanisms at different temperatures.

Conclusion

In this study, the effects of hydrogen and temperature on the impact response of Al 7075 alloy were investigated. Impact tests were conducted at a wide range of temperatures (from −45 °C to 100 °C). Corresponding microstructural investigations were carried out via SEM. Therefore, HE susceptibility of Al 7075 alloy has been investigated under impact loading. From the work presented herein the following conclusions can be drawn:

1) HE was observed under impact loading. In particular, the coexistence of HELP + HEDE mechanisms was observed depending on the testing temperature. This observation was proven via microstructural observations and MD modeling. In particular, with the aid of MD modeling, it was seen that hydrogen decreased the cohesive energy and enhanced the average dislocation mobility.
2) The crack propagated through at almost 45° to the direction of the impact loading at low temperatures, whereas hydrogen changed the crack propagation mode from ductile transgranular to brittle intergranular at elevated temperatures.
3) Hydrogen degraded the impact response of Al 7075 alloy in terms of absorbed energy, contact force, and corresponding toughness.
4) Hydrogen decreased the time for fracture under impact loading regardless of the testing temperature.

Declaration of competing interest

The authors declare that they have no known competing financial interests or personal relationships that could have appeared to influence the work reported in this paper.

Appendix A. Supplementary data

Supplementary data related to this article can be found at https://doi.org/10.1016/j.ijhydene.2020.06.241.

REFERENCES

[1] Bal B. Determination of material response and optimization of johnson-cook damage parameters of aluminium 7075 alloy. Selcuk Univ J Eng ,Science Technol 2018;6:343–54. https://doi.org/10.15317/Scitech.2018.137.

[2] Arockiasamy A, Eliezer D, Wang PT, Horstemeyer MF, King RL. Effect of cathodic charging on Al-32Si-2Cu alloy in acidic solution. Mater Res 2010;13:361–7. https://doi.org/10.1590/s1516-14392010000300014.

[3] Kumar PV, Reddy GM, Rao KS. Microstructure, mechanical and corrosion behavior of high strength AA7075 aluminium alloy friction stir welds – effect of post weld heat treatment. Def Technol 2015;11:362–9. https://doi.org/10.1016/j.dt.2015.04.003.

[4] Senthil K, Iqbal MA, Chandel PS, Gupta NK. Study of the constitutive behavior of 7075-T651 aluminum alloy. Int J Impact Eng 2017;108:171–90. https://doi.org/10.1016/j.ijimpeng.2017.05.002.

[5] Deya S, Chattoraja I, Sivaprasada S. Effect of hydrogen on mechanical degradation and fatigue in 7075 aluminium alloy with in-situ hydrogenation. Procedia Eng 2015;114:461–9. https://doi.org/10.1016/j.proeng.2015.08.093.

[6] Tajally M, Huda Z, Masjuki HH. A comparative analysis of tensile and impact-toughness behavior of cold-worked and annealed 7075 aluminum alloy. Int J Impact Eng 2010;37:425–32. https://doi.org/10.1016/j.ijimpeng.2009.08.009.

[7] Davis JR. Aluminum and aluminum alloys. Light Met Alloy 2001:351–416. https://doi.org/10.1361/autb2001p351.

[8] Rometsch PA, Zhang Y, Knight S. Heat treatment of 7xxx series aluminium alloys - some recent developments. Trans Nonferrous Met Soc China English Ed 2014;24:2003–17. https://doi.org/10.1016/S1003-6326(14)63306-9.

[9] Leacock AG, Howe C, Brown D, Lademo O-G, Deering A. Evolution of mechanical properties in a 7075 Al-alloy subject to natural ageing. Mater Des 2013;49:160–7. https://doi.org/10.1016/j.matdes.2013.02.023.

[10] Ghosh A, Ghosh M, Shankar G. On the role of precipitates in controlling microstructure and mechanical properties of Ag and Sn added 7075 alloys during artificial ageing. Mater Sci Eng A 2018;738:399–411. https://doi.org/10.1016/j.msea.2018.09.109.

[11] Aoba T, Kobayashi M, Miura H. Effects of aging on mechanical properties and microstructure of multi-directionally forged 7075 aluminum alloy. Mater Sci Eng A 2017;700:220–5. https://doi.org/10.1016/j.msea.2017.06.017.

[12] Panigrahi SK, Jayaganthan R. Effect of ageing on microstructure and mechanical properties of bulk, cryorolled, and room temperature rolled Al 7075 alloy. J Alloys Compd 2011;509:9609–16. https://doi.org/10.1016/j.jallcom.2011.07.028.

[13] Takano N. Hydrogen diffusion and embrittlement in 7075 aluminum alloy. Mater Sci Eng A 2008;483–484:336–9. https://doi.org/10.1016/j.msea.2006.08.144.

[14] Scully JR, Young GA, Smith SW. Hydrogen embrittlement of aluminum and aluminum-based alloys. Gaseous Hydrog Embrittlement Mater Energy Technol Probl Its Characterisation Eff Part Alloy Classes 2012;2:707–68. https://doi.org/10.1533/9780857093899.3.707.

[15] Rao ACU, Vasu V, Govindaraju M, Srinadh KVS. Stress corrosion cracking behaviour of 7xxx aluminum alloys: a literature review. Trans Nonferrous Met Soc China English Ed 2016;26:1447–71. https://doi.org/10.1016/S1003-6326(16)64220-6.

[16] Bochkaryova AV, Li YV, Barannikova SA, Zuev LB. The effect of hydrogen embrittlement on the mechanical properties of aluminum alloy. IOP Conf Ser Mater Sci Eng 2015;71. https://doi.org/10.1088/1757-899X/71/1/012057.

[17] Bal B. Numerical investigation of the role of volumetric transformation strain on the relaxation stress and the corresponding hydrogen interstitial concentration in niobium matrix. Adv Mater Sci Eng 2017;2017. https://doi.org/10.1155/2017/2036516.

[18] Dwivedi SK, Vishwakarma M. Hydrogen embrittlement in different materials: a review. Int J Hydrogen Energy 2018;43:21603–16. https://doi.org/10.1016/j.ijhydene.2018.09.201.

[19] Dwivedi SK, Vishwakarma M. Effect of hydrogen in advanced high strength steel materials. Int J Hydrogen Energy 2019;44:28007–30. https://doi.org/10.1016/j.ijhydene.2019.08.149.

[20] Tuğluca IB, Koyama M, Bal B, Canadinc D, Akiyama E, Tsuzaki K. High-concentration carbon assists plasticity-driven hydrogen embrittlement in a Fe-high Mn steel with a relatively high stacking fault energy. Mater Sci Eng A 2018;717:78–84. https://doi.org/10.1016/j.msea.2018.01.087.

[21] Fournier L, Delafosse D, Magnin T. Cathodic hydrogen embrittlement in alloy 718. Mater Sci Eng A 1999;269:111–9. https://doi.org/10.1016/S0921-5093(99)00167-7.

[22] Ehrlin N, Bjerkén C, Fisk M. Cathodic hydrogen charging of Inconel 718. AIMS Mater Sci 2016;3:1350–64. https://doi.org/10.3934/matersci.2016.4.1350.

[23] Wasim M, Djukic MB. Hydrogen embrittlement of low carbon structural steel at macro-, micro- and nano-levels. Int J Hydrogen Energy 2019. https://doi.org/10.1016/j.ijhydene.2019.11.070.

[24] Li X, Zhang J, Fu Q, Akiyama E, Song X, Wang Y, et al. Tensile mechanical properties and fracture behaviors of nickel-based superalloy 718 in the presence of hydrogen. Int J Hydrogen Energy 2018;43:20118–32. https://doi.org/10.1016/j.ijhydene.2018.08.179.

[25] Merson ED, Myagkikh PN, Poluyanov VA, Merson DL, Vinogradov A. Quasi-cleavage hydrogen-assisted cracking path investigation by fractographic and side surface observations. Eng Fract Mech 2019;214:177–93. https://doi.org/10.1016/j.engfracmech.2019.04.042.

[26] Dadfarnia M, Novak P, Ahn DC, Liu JB, Sofronis P, Johnson DD, et al. Recent advances in the study of structural materials compatibility with hydrogen. Adv Mater 2010;22:1128–35. https://doi.org/10.1002/adma.200904354.

[27] Barnoush A, Vehoff H. Recent developments in the study of hydrogen embrittlement: hydrogen effect on dislocation nucleation. Acta Mater 2010;58:5274–85. https://doi.org/10.1016/j.actamat.2010.05.057.

[28] Merson E, Danilov V, Merson D, Vinogradov A. Confocal laser scanning microscopy: the technique for quantitative fractographic analysis. Eng Fract Mech 2017;183:147–58. https://doi.org/10.1016/j.engfracmech.2017.04.026.

[29] Bal B, Sahin I, Uzun A, Canadinc D. A new venue toward predicting the role of hydrogen embrittlement on metallic

materials. Metall Mater Trans A Phys Metall Mater Sci 2016;47:5409–22. https://doi.org/10.1007/s11661-016-3708-z.
[30] Birnbaum HK, Sofronis P. Hydrogen-enhanced localized plasticity-a mechanism for hydrogen-related fracture. Mater Sci Eng A 1994;176:191–202. https://doi.org/10.1016/0921-5093(94)90975-X.
[31] Beachem CD. A new model for hydrogen-assisted cracking (hydrogen "embrittlement"). Metall Trans 1972;3:437–51. https://doi.org/10.1007/BF02642048.
[32] Oriani RA, Josephic PH. Equilibrium and kinetic studies of the hydrogen-assisted cracking of steel. Acta Metall 1977;25:979–88. https://doi.org/10.1016/0001-6160(77)90126-2.
[33] Djukic MB, Bakic GM, Sijacki Zeravcic V, Sedmak A, Rajicic B. The synergistic action and interplay of hydrogen embrittlement mechanisms in steels and iron: localized plasticity and decohesion. Eng Fract Mech 2019;216:106528. https://doi.org/10.1016/j.engfracmech.2019.106528.
[34] Hirth JP, Carnahan B. Hydrogen adsorption at dislocations and cracks in Fe. Acta Metall 1978;26:1795–803. https://doi.org/10.1016/0001-6160(78)90092-5.
[35] Kappes M, Iannuzzi M, Carranza RM. Hydrogen embrittlement of magnesium and magnesium alloys: a review. J Electrochem Soc 2013;160:168–78. https://doi.org/10.1149/2.023304jes.
[36] Su H, Toda H, Masunaga R, Shimizu K, Gao H, Sasaki K, et al. Influence of hydrogen on strain localization and fracture behavior in Al–Zn–Mg–Cu aluminum alloys. Acta Mater 2018;159:332–43. https://doi.org/10.1016/j.actamat.2018.08.024.
[37] Petroyiannis PV, Kermanidis AT, Papanikos P, Pantelakis SG. Corrosion-induced hydrogen embrittlement of 2024 and 6013 aluminum alloys. Theor Appl Fract Mech 2004;41:173–83. https://doi.org/10.1016/j.tafmec.2003.11.014.
[38] Gupta C, Toda H, Fujioka T, Kobayashi M, Hoshino H, Uesugi K, et al. State of 3-D micro-damage in hydrogen redistributed regions of precharged high strength aluminium alloy. Corros Sci 2016;111:26–38. https://doi.org/10.1016/j.corsci.2016.04.050.
[39] Ambat R, Dwarakadasa ES. Effect of hydrogen in aluminium and aluminium alloys: a review. Bull Mater Sci 1996;19:103–14. https://doi.org/10.1007/BF02744792.
[40] Su H, Toda H, Shimizu K, Uesugi K, Takeuchi A, Watanabe Y. Assessment of hydrogen embrittlement via image-based techniques in Al–Zn–Mg–Cu aluminum alloys. Acta Mater 2019;176:96–108. https://doi.org/10.1016/j.actamat.2019.06.056.
[41] Alexopoulos ND, Charalampidou C, Skarvelis P, Kourkoulis SK. Synergy of corrosion-induced micro-cracking and hydrogen embrittlement on the structural integrity of aluminium alloy (Al-Cu-Mg) 2024. Corros Sci 2017;121:32–42. https://doi.org/10.1016/j.corsci.2017.03.001.
[42] Dey S, Chattoraj I. Interaction of strain rate and hydrogen input on the embrittlement of 7075 T6 Aluminum alloy. Mater Sci Eng A 2016;661:168–78. https://doi.org/10.1016/j.msea.2016.03.010.
[43] Pouillier E, Gourgues AF, Tanguy D, Busso EP. A study of intergranular fracture in an aluminium alloy due to hydrogen embrittlement. Int J Plast 2012;34:139–53. https://doi.org/10.1016/j.ijplas.2012.01.004.
[44] Zeides F, Roman I. Study of hydrogen embrittlement in aluminium alloy 2024 in the longitudinal direction. Mater Sci Eng A 1990;125:21–30. https://doi.org/10.1016/0921-5093(90)90248-2.
[45] Nguyen D, Thompson AW, Bernstein IM. Microstructural effects on hydrogen embrittlement in a high purity 7075 aluminum alloy. Acta Metall 1987;35:2417–25. https://doi.org/10.1016/0001-6160(87)90139-8.
[46] Shimizu K, Toda H, Fujihara H, Hirayama K, Uesugi K, Takeuchi A. Hydrogen partitioning behavior and related hydrogen embrittlement in Al-Zn-Mg alloys. Eng Fract Mech 2019;216. https://doi.org/10.1016/j.engfracmech.2019.106503.
[47] Ogawa Y, Kim D, Matsunaga H, Matsuoka S. Evaluation of the compatibility of high-strength aluminum alloy 7075-T6 to high-pressure gaseous hydrogen environments. Am Soc Mech Eng Press Vessel Pip Div PVP 2018;6B:1–9. https://doi.org/10.1115/pvp2018-84321.
[48] Burns JT, Jones JJ, Thompson AD, (Warner) Locke JS. Fatigue crack propagation of aerospace aluminum alloy 7075-T651 in high altitude environments. Int J Fatig 2018;106:196–207. https://doi.org/10.1016/j.ijfatigue.2017.09.017.
[49] Bal B, Koyama M, Canadinc D, Gerstein G, Maier HJ, Tsuzaki K. On the utility of crystal plasticity modeling to uncover the individual roles of microdeformation mechanisms on the work hardening response of Fe-23Mn-0.5C TWIP steel in the presence of hydrogen. J Eng Mater Technol Trans ASME 2018;140:1–13. https://doi.org/10.1115/1.4038801.
[50] Kim KS, Kang JH, Kim SJ. Nitrogen effect on hydrogen diffusivity and hydrogen embrittlement behavior in austenitic stainless steels. Scr Mater 2020;184:70–3. https://doi.org/10.1016/j.scriptamat.2020.03.038.
[51] El-Amoush AS. Investigation of corrosion behaviour of hydrogenated 7075-T6 aluminum alloy. J Alloys Compd 2007;443:171–7. https://doi.org/10.1016/j.jallcom.2006.12.045.
[52] El-Amoush AS. An investigation of hydrogen-induced hardening in 7075-T6 aluminum alloy. J Alloys Compd 2008;465:497–501. https://doi.org/10.1016/j.jallcom.2007.10.126.
[53] Gupta C, Toda H, Fujioka T, Kobayashi M, Hoshino H, Uesugi K, et al. Quantitative tomography of hydrogen precharged and uncharged Al-Zn-Mg-Cu alloy after tensile fracture. Mater Sci Eng A 2016;670:300–13. https://doi.org/10.1016/j.msea.2016.06.011.
[54] Najam H, Koyama M, Bal B, Akiyama E, Tsuzaki K. Strain rate and hydrogen effects on crack growth from a notch in a Fe-high-Mn steel containing 1.1 wt% solute carbon. Int J Hydrogen Energy 2020;45:1125–39. https://doi.org/10.1016/j.ijhydene.2019.10.227.
[55] Ambriz RR, Jaramillo D, García C, Curiel FF. Fracture energy evaluation on 7075-T651 aluminum alloy welds determined by instrumented impact pendulum. Trans Nonferrous Met Soc China (English Ed) 2016;26:974–83. https://doi.org/10.1016/S1003-6326(16)64157-2.
[56] Das P, Jayaganthan R, Singh IV. Tensile and impact-toughness behaviour of cryorolled Al 7075 alloy. Mater Des 2011;32:1298–305. https://doi.org/10.1016/j.matdes.2010.09.026.
[57] Rotella G, Dillon OW, Umbrello D, Settineri L, Jawahir IS. Finite element modeling of microstructural changes in turning of AA7075-T651 Alloy. J Manuf Process 2013;15:87–95. https://doi.org/10.1016/j.jmapro.2012.09.005.
[58] Zhao Q, Liu Z, Li S, Huang T, Xia P, Lu L. Evolution of the Brass texture in an Al-Cu-Mg alloy during hot rolling. J Alloys Compd 2017;691:786–99. https://doi.org/10.1016/j.jallcom.2016.08.322.
[59] Jayaganthan R, Brokmeier HG, Schwebke B, Panigrahi SK. Microstructure and texture evolution in cryorolled Al 7075 alloy. J Alloys Compd 2010;496:183–8. https://doi.org/10.1016/j.jallcom.2010.02.111.
[60] Yamada H, Tsurudome M, Miura N, Horikawa K, Ogasawara N. Ductility loss of 7075 aluminum alloys affected by interaction of hydrogen, fatigue deformation, and strain rate. Mater Sci Eng A 2015;642:194–203. https://doi.org/10.1016/j.msea.2015.06.084.

[61] Xia SQ, Gao MC, Zhang Y. Abnormal temperature dependence of impact toughness in AlxCoCrFeNi system high entropy alloys. Mater Chem Phys 2017;210:213–21. https://doi.org/10.1016/j.matchemphys.2017.06.021.
[62] Chao YJ, Ward JD, Sands RG. Charpy impact energy, fracture toughness and ductile-brittle transition temperature of dual-phase 590 Steel. Mater Des 2007;28:551–7. https://doi.org/10.1016/j.matdes.2005.08.009.
[63] Bal B, Gumus B, Gerstein G, Canadinc D, Maier HJ. On the micro-deformation mechanisms active in high-manganese austenitic steels under impact loading. Mater Sci Eng A 2015;632:29–34. https://doi.org/10.1016/j.msea.2015.02.054.
[64] Gumus B, Bal B, Gerstein G, Canadinc D, Maier HJ, Guner F, et al. Twinning activities in high-Mn austenitic steels under high-velocity compressive loading. Mater Sci Eng A 2015;648:104–12. https://doi.org/10.1016/j.msea.2015.09.045.
[65] Nguyen LTH, Hwang JS, Kim MS, Kim JH, Kim SK, Lee JM. Charpy impact properties of hydrogen-exposed 316l stainless steel at ambient and cryogenic temperatures. Metals 2019;9. https://doi.org/10.3390/met9060625.
[66] Llnderoth S. Hydrogen diffusivity in aluminium. Phil Mag Lett 1988;57:229–34. https://doi.org/10.1080/09500838808214712.
[67] Padhy GK, Ramasubbu V, Parvathavarthini N, Wu CS, Albert SK. Influence of temperature and alloying on the apparent diffusivity of hydrogen in high strength steel. Int J Hydrogen Energy 2015;40:6714–25. https://doi.org/10.1016/j.ijhydene.2015.03.153.
[68] Zhou C, Hong Y, Zhang L, An B, Zheng J, Chen X. Abnormal effect of nitrogen on hydrogen gas embrittlement of austenitic stainless steels at low temperatures. Int J Hydrogen Energy 2016;41:13777–85. https://doi.org/10.1016/j.ijhydene.2016.06.100.
[69] Hirth JP. Effects of hydrogen on the properties of iron and steel. Metall Trans A 1980;11:861–90. https://doi.org/10.1007/BF02654700.
[70] Merson E, Kudrya AV, Trachenko VA, Merson D, Danilov V, Vinogradov A. Quantitative characterization of cleavage and hydrogen-assisted quasi-cleavage fracture surfaces with the use of confocal laser scanning microscopy. Mater Sci Eng A 2016;665:35–46. https://doi.org/10.1016/j.msea.2016.04.023.
[71] Kumar A, Roberts SG, Wilkinson AJ. Low-temperature fracture mechanisms in a spheroidised reactor pressure vessel steel. Int J Fract 2007;144:121–9. https://doi.org/10.1007/s10704-007-9084-3.
[72] Bal B, Koyama M, Gerstein G, Maier HJ, Tsuzaki K. Effect of strain rate on hydrogen embrittlement susceptibility of twinning-induced plasticity steel pre-charged with high-pressure hydrogen gas. Int J Hydrogen Energy 2016;41:15362–72. https://doi.org/10.1016/j.ijhydene.2016.06.259.
[73] Depover T, Pérez Escobar D, Wallaert E, Zermout Z, Verbeken K. Effect of hydrogen charging on the mechanical properties of advanced high strength steels. Int J Hydrogen Energy 2014;39:4647–56. https://doi.org/10.1016/j.ijhydene.2013.12.190.
[74] Hong HL, Wang Q, Dong C, Liaw PK. Understanding the Cu-Zn brass alloys using a short-range-order cluster model: significance of specific compositions of industrial alloys. Sci Rep 2014;4. https://doi.org/10.1038/srep07065.
[75] Adlakha I, Solanki KN. Critical assessment of hydrogen effects on the slip transmission across grain boundaries in α-Fe. Proc R Soc A Math Phys Eng Sci 2016;472. https://doi.org/10.1098/rspa.2015.0617.
[76] Koyama M, Akiyama E, Sawaguchi T, Raabe D, Tsuzaki K. Hydrogen-induced cracking at grain and twin boundaries in an Fe-Mn-C austenitic steel. Scr Mater 2012;66:459–62. https://doi.org/10.1016/j.scriptamat.2011.12.015.
[77] Koyama M, Akiyama E, Tsuzaki K. Hydrogen embrittlement in a Fe-Mn-C ternary twinning-induced plasticity steel. Corros Sci 2012;54:1–4. https://doi.org/10.1016/j.corsci.2011.09.022.
[78] Djukic MB, Zeravcic VS, Bakic G, Sedmak A, Rajicic B. Hydrogen embrittlement of low carbon structural steel. Procedia Mater Sci 2014;3:1167–72. https://doi.org/10.1016/j.mspro.2014.06.190.
[79] Djukic MB, Bakic GM, Zeravcic VS, Rajicic B, Sedmak A, Mitrovic R, et al. Towards a unified and practical industrial model for prediction of hydrogen embrittlement and damage in steels. Procedia Struct Integr 2016;2:604–11. https://doi.org/10.1016/j.prostr.2016.06.078.
[80] Martin ML, Fenske JA, Liu GS, Sofronis P, Robertson IM. On the formation and nature of quasi-cleavage fracture surfaces in hydrogen embrittled steels. Acta Mater 2011;59:1601–6. https://doi.org/10.1016/j.actamat.2010.11.024.
[81] Hassan Sk M, Overfelt RA. Microstructurally mediated changes in fracture characteristics for electrochemically hydrogenated 4340 steel. Mater Perform Charact 2015;4:68–83. https://doi.org/10.1520/mpc20140026.
[82] Server W, Wullaert R, Sheckherd J. Evaluation of current procedures for dynamic fracture-toughness testing. Flaw Growth Fract 1977:446–61. https://doi.org/10.1520/stp35554s.
[83] Ma N, Park T, Kim D, Kim C, Chung K. Numerical and experimental evaluation of the impact performance of advanced high-strength steel sheets based on a damage model. Met Mater Int 2010;16:427–39. https://doi.org/10.1007/s12540-010-0613-7.
[84] Scully JR, Young GA, Smith SW. Hydrogen solubility, diffusion and trapping in high purity aluminum and selected Al-base alloys. Mater Sci Forum 2000;331:1583–600. https://doi.org/10.4028/www.scientific.net/msf.331-337.1583.
[85] Anyalebechi PN. Critical review of reported values of hydrogen diffusion in solid and liquid aluminum and its alloys. TMS Light Met 2003:857–72.
[86] Yarımpabuç D, Celebi K, Çalık A, Horpan MS. Exact analysis of hydrogen induced stress in metal solid sphere. Int J Hydrogen Energy 2018;43:18053–8. https://doi.org/10.1016/j.ijhydene.2018.04.019.
[87] Stashchuk M, Dorosh M. Analytical evaluation of hydrogen induced stress in metal. Int J Hydrogen Energy 2017;42:6394–400. https://doi.org/10.1016/j.ijhydene.2017.01.022.
[88] Ko WS, Shim JH, Lee BJ. Atomistic modeling of the Al-H and Ni-H systems. J Mater Res 2011;26:1552–60. https://doi.org/10.1557/jmr.2011.95.
[89] Stukowski A, Bulatov VV, Arsenlis A. Automated identification and indexing of dislocations in crystal interfaces. Model Simul Mater Sci Eng 2012;20. https://doi.org/10.1088/0965-0393/20/8/085007.
[90] Stukowski A. Visualization and analysis of atomistic simulation data with OVITO-the Open Visualization Tool. Model Simul Mater Sci Eng 2010;18. https://doi.org/10.1088/0965-0393/18/1/015012.
[91] Verners O, Psofogiannakis G, van Duin ACT. Comparative molecular dynamics study of fcc-Al hydrogen embrittlement. Corros Sci 2015;98:40–9. https://doi.org/10.1016/j.corsci.2015.05.008.
[92] Ko WS, Jeon JB, Shim JH, Lee BJ. Origin of hydrogen embrittlement in vanadium-based hydrogen separation membranes. Int J Hydrogen Energy 2012;37:13583–93. https://doi.org/10.1016/j.ijhydene.2012.06.075.
[93] Matsumoto R, Taketomi S, Matsumoto S, Miyazaki N. Atomistic simulations of hydrogen embrittlement. Int J Hydrogen Energy 2009;34:9576–84. https://doi.org/10.1016/j.ijhydene.2009.09.052.
[94] Yu H, Cocks ACF, Tarleton E. Simulating hydrogen in fcc materials with discrete dislocation plasticity. Int J Hydrogen Energy 2020;45:14565–77. https://doi.org/10.1016/j.ijhydene.2020.01.118.